

## STELLAR JETS WITH INTRINSICALLY VARIABLE SOURCES

A. C. RAGA,<sup>1</sup> J. CANTÓ,<sup>2</sup> L. BINETTE,<sup>1</sup> AND N. CALVET<sup>3</sup>*Received 1990 March 22; accepted 1990 May 30*

## ABSTRACT

New observational evidence indicates that the sources of stellar jets might be intrinsically variable. In some cases, the radial velocity of the jets shows strong variations with position, which can be interpreted as evidence for a variable ejection velocity. Some jets show discontinuous jumps in the radial velocity (as a function of position along the jet) and also show two or more well-aligned bow shock-like structures. Such structures can be interpreted as evidence for multiple outflow episodes from the jet source.

In this paper, we present simplified models for jets from sources with time-dependent velocities. We find that the relaxation of the assumption of a time-independent source (an assumption common to most of the jet models which have been previously calculated) allows us to explain in a very straightforward way the complex position-velocity diagrams and multiple bow shock structures observed in some stellar jets.

We present both analytic and numerical models for jets with variable velocity sources. We carry out a comparison with previously published observations of the HH 46/47 jet which illustrates the very promising characteristics of these models. From this comparison, we show how the velocity variations observed along a jet can be used to reconstruct the past time variability of the source. This technique is potentially very interesting for future studies of the mechanism by which stellar jets are produced.

*Subject headings:* hydrodynamics — stars: pre—main—sequence

## I. INTRODUCTION

The emission spectrum of Herbig-Haro objects appears to come from the recombination regions of shock waves (as first suggested by Schwartz 1975) produced by the interaction of a high-velocity outflow (from a young star) with the surrounding environment. The precise nature of this interaction has been the focus of recent theoretical models.

At this time, a considerable amount of progress in understanding the Herbig-Haro (HH) objects classified as “stellar jets” has been made. Stellar jets show a well-organized, linear structure, extending from close to the outflow source to a sometimes well-defined “head” (in contrast to other Herbig-Haro objects, which many times show an apparently somewhat chaotic spatial structure). This structure was first observed in the HH 34 system (Reipurth *et al.* 1986; Bührke, Mundt, and Ray 1988) but now has been detected in several other objects (see, e.g., the review of Reipurth 1989*a*). The models of stellar jets have concentrated on three different aspects of this kind of flow:

1.—The mechanisms by which collimated outflows can be produced in the near environment of the source (e.g., Cantó 1980; Königl 1982; Cantó, Tenorio-Tangle, and Różyńska 1987; Raga and Cató 1989*a, b*);

2.—The excitation of internal shocks in nonadiabatic jetlike flows (e.g., Königl 1982; Silvestro *et al.* 1987; Bührke, Mundt, and Ray 1988; Cantó, Raga, and Binette 1989; Tenorio-Tagle 1989; Raga, Binette, and Cantó 1990; Blondin, Fryxell, and Königl 1990); and

3.—The interaction of the “head” of a stellar jet with the surrounding environment (Raga 1988; Hartigan 1989; Blondin, Königl, and Fryxell 1989).

These models have been calculated under widely different approximations and simplifying assumptions. However, an

assumption common to all of these models is that the outflow source has been “turned on” at some time in the past and has thereafter been time-independent (i.e., the radius, velocity, temperature and density of the jet close to the source are assumed to be constant with time). This particular assumption appears to be challenged by some recent observational results.

Recent deep, high resolution long-slit spectra of HH 34, HH 83, and HH 46/47 (Reipurth 1989*a, b*; Heathcote and Reipurth 1990) show that the radial velocity of the emitting material (as observed in the red [S II] lines) increases with increasing distance from the source (increases of up to ~50% in the radial velocity are observed). As discussed by Reipurth (1989*b*), this result could be interpreted as (1) evidence for a gradual “bending” of the jet toward the observer, (2) an acceleration of the jet with increasing distance from the source, or (3) a gradual decrease of the velocity of the outflow (close to the position of the source) with time.

The first of these possibilities is in principle sound, but the fact that the jets appear to be quite straight in the plane of the sky makes this explanation somewhat unlikely.

The second of these scenarios appears to be impossible, at least for purely hydrodynamic jets. The fact that the observed jets have Mach numbers of order  $M \sim 10$  close to the source means that the possible acceleration of the jet due to pressure forces is minimal (and could not even account for velocity variations an order of magnitude lower than the observed values of ~50%, as was pointed out by Reipurth 1989*b*). Internal shocks in jets (as described, e.g., by Blondin, Fryxell, and Königl 1990; Cantó, Raga, and Binette 1989) produce expansions and recollimations of the flow which do result in variations of the jet velocity (along the symmetry axis). For flows with Mach numbers of 10 or higher, however, these variations are very small (Biro 1990) and cannot account for the observed velocity changes. With these arguments, we can rule out the conjecture that the observed velocity variations are a result of a hydrodynamical acceleration of the jet. However, an MHD jet with an initially low Alfvénic Mach number (but high hydro-

<sup>1</sup> Canadian Institute for Theoretical Astrophysics.

<sup>2</sup> Instituto de Astronomía, Universidad Nacional Autónoma de México.

<sup>3</sup> Centro de Investigaciones de Astronomía.

dynamic Mach number) in principle might show accelerations such as the observed ones.

In this paper, we explore the third of the scenarios proposed above. We study jets from a source with an intrinsically time-dependent ejection velocity. In the context of extragalactic jets, this problem has been described by Rees (1978) and studied numerically by Wilson (1984). The numerical models of Wilson (1984) show that jets from time-dependent sources develop a structure of successive "working surfaces," separated by regions of undisturbed jet flow. We present simplified, one-dimensional models for these flows, with which we can explore different possible flow parameters. These models produce predictions that can easily be compared with the observed position-dependent jet velocities, and also with the "multiple-bow shock" structures observed in some stellar jets (which show relatively large proper motions, see Reipurth 1989a).

In § II, we describe the general properties of jets from variable velocity sources, and in § III, we describe numerical calculations of jets with periodically varying sources. We show a comparison of these results with observations of the HH 46/47 jet in § IV.

## II. EFFECTS OF SOURCE VARIATIONS ON HIGH MACH NUMBER JETS

### a) Criterion for the Formation of Discontinuities

We will consider an initially steady, high Mach number jet in pressure equilibrium with its environment. If we introduce a perturbation on the jet velocity at the position of the source, there will be an adjustment of the downstream region of the jet to the new source conditions. This adjustment can take place either through continuous rarefaction or compression waves, or through one or more shock waves. A criterion for deciding which of these two possibilities actually occurs can be obtained in the following way.

Let us consider a jet injected with a velocity:

$$u_0(t) = U_0 ; \quad t < 0 , \quad (1a)$$

$$u_0(t) = U_0 + \alpha t ; \quad t \geq 0 , \quad (1b)$$

where  $u_0(t)$  is the time-dependent injection velocity,  $U_0 = u_0(t=0)$  is the initial jet velocity, and  $\alpha = (du_0/dt)_{t=0}$ , which we assume to be greater than zero. If the Mach number of the jet is very high, the effect of pressure forces along the jet axis will be negligible, and the jet can be approximated with a ballistic description.

Two parcels ejected at times  $t = 0$  and  $t = \Delta t$  have velocities  $U_0$  and  $U_0 + \Delta t \times (du_0/dt)_{t=0}$ , respectively. If  $\alpha = (du_0/dt)_{t=0}$  is greater than zero, these two parcels will coincide in position after a time:

$$t_s = \left[ \frac{U_0}{(du_0/dt)_{t=0}} \right] + \Delta t \xrightarrow{\Delta t \rightarrow 0} \frac{U_0}{(du_0/dt)_{t=0}} . \quad (2)$$

The distance from the source at which the two parcels will coincide in position is (in the limit of small  $\Delta t$ ):

$$d_s = U_0 \times t_s = \frac{U_0^2}{(du_0/dt)_{t=0}} . \quad (3)$$

In other words, a configuration of an initially constant velocity jet with a source that starts to increase in velocity as described by equation (1), will develop a discontinuity after a time  $t_s$  (as given by eq. [2]). The initial location of this discontinuity will be at a distance  $d_s$  (see eq. [3]) downstream from

the injection point of the jet. On the other hand, for sources with velocities decreasing with time (i.e., sources with  $\alpha = du_0/dt < 0$ ; see eq. [1]), equation (3) gives a negative distance, indicating that no discontinuities are formed.

This criterion for the formation of discontinuities (see eq. [3]) is of somewhat limited application because of our assumptions. We have assumed that the jet effectively has zero temperature (in that we have completely neglected the effects of pressure forces). The criterion for the formation of a discontinuity for the case with a nonzero sound speed can be obtained replacing  $U_0$  (in eqs. [2] and [3]) by  $2(U_0 + c_0)/(\gamma + 1)$  (where  $\gamma$  is the specific heat ratio and  $c_0$  is the initial sound speed of the flow; see Landau and Lifshitz 1987, § 94). For the case of an isothermal (i.e.,  $\gamma = 1$ ) flow with  $c_0 \ll U_0$ , equations (2) and (3) are recovered.

Highly supersonic perturbations (i.e., perturbations with  $\Delta u_0/c_0 \gg 1$ , where  $c_0$  is the initial jet sound speed) will produce a discontinuity at the time and distance from the source given by equations (2) and (3), respectively. In the following section, we will describe the general structure of such discontinuities.

### b) Structure of the Discontinuity

In the previous section, we have described how supersonic perturbations in the injection velocity lead to the formation of internal discontinuities in a jet. We will now describe the general structure of these discontinuities, limiting ourselves to the case of highly supersonic jets.

In the numerical simulations of Wilson (1984), the discontinuities that result from the source velocity variations have a two-shock structure. In Figure 1, we show a schematic diagram of such a configuration.

The jet is characterized by an upstream velocity  $u_1$ , and a lower downstream velocity  $u_2 < u_1$ . In the highly supersonic case (where  $u_1 - u_2 \gg c_s$ , the local sound speed), two shocks are formed: an "upstream" (i.e., toward the source), and a "downstream" (i.e., away from the source) shock. This structure resembles the "working surface" of a jet (see, e.g., the review of Dyson 1987).

The velocity with which this "internal working surface" moves inside the jet is determined by the balance of upstream

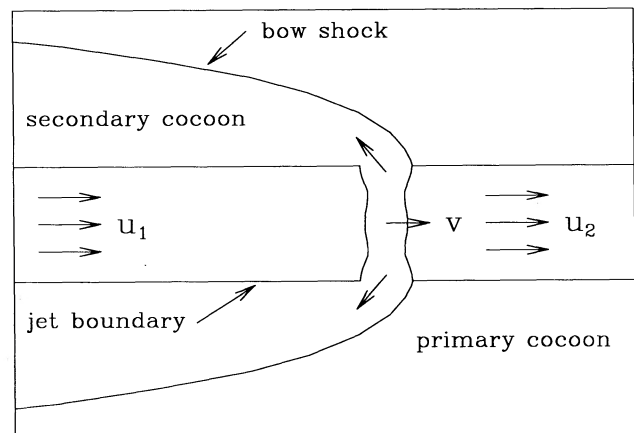


FIG. 1.—Schematic diagram showing the structure of internal working surfaces in jets. The working surface moves with a velocity  $v$ , that satisfies  $u_1 > v > u_2$  (where  $u_1$  and  $u_2$  are the upstream and downstream flow velocities, respectively). The high pressure between the two shocks of the working surface drives out material sideways, and the interaction of the ejected gas with the surrounding environment forms a bow shock (see the discussion in § IIb).

and downstream ram pressures:

$$\rho_1(u_1 - v)^2 = \rho_2(v - u_2)^2, \quad (4)$$

where  $v$  is the velocity of the working surface,  $\rho_1$  and  $u_1$  are the upstream density and velocity, and  $\rho_2$  and  $u_2$  are the corresponding downstream parameters (see Fig. 1). Solving for the velocity of the working surface  $v$ , we obtain

$$v = \frac{\beta u_1 + u_2}{1 + \beta}, \quad (5)$$

where  $\beta = (\rho_1/\rho_2)^{1/2}$ .

The parameter  $\beta$  is in principle a free parameter of the problem. However, pressure-balanced stellar jets are likely to be approximately isothermal (with a temperature of  $\sim 10^3$ – $10^4$  K; see, e.g., Raga, Binette, and Cantó 1990). This (together with the condition of pressure balance with a uniform environment) would lead to the conclusion that  $\beta = (\rho_1/\rho_2)^{1/2} \sim 1$  for pressure-matched stellar jets.

However, a jet in which this pressure balance condition is satisfied will have a position-dependent radius. In particular, the jet radius will present a sudden change at the position of the internal working surface, resulting in a shock structure that would be considerably more complex than the one depicted in Figure 1. The ram pressure balance (eq. [4]) will then only be satisfied in the region close to the axis of symmetry of the flow, and the motion of the working surface as a whole might not be properly described by equation (5). Nonetheless, the  $\beta = 1$  case might be applicable at least for some jet flows. For  $\beta = 1$ , equation (5) simplifies to

$$v = \frac{1}{2}(u_1 + u_2). \quad (6)$$

The shock velocity (i.e., the velocity of the preshock flow with respect to the velocity of the working surface) of the upstream and downstream facing shocks (both have the same shock velocity  $v_s$ ) is then given by

$$v_s = \frac{1}{2}(u_1 - u_2). \quad (7)$$

The maximum pressure in the working surface (obtained on the axis of symmetry) is

$$P_{\max} = \rho \left( \frac{u_1 - u_2}{2} \right)^2, \quad (8)$$

where  $\rho$  is the density of the jet (as we have argued above, the upstream and downstream regions have similar densities).

For the highly supersonic perturbations that we are considering, the on-axis pressure  $P_{\max}$  (see eq. [8]) is much larger than the environmental pressure. This overpressure in the working surface will drive material outward, forming a “secondary cocoon” around the jet (see Fig. 1). This secondary cocoon drives a bow shock into the “primary cocoon” (which is formed by the leading working surface of the jet), producing a configuration that resembles the head of a jet. The main difference between the internal working surfaces (described above) and the head of a jet, is the absence of the strong on-axis shocks which are present in the case of the head of a jet. In the internal working surfaces, the on-axis shocks are driven into the downstream part of the jet (which is moving at a velocity  $u_2$  away from the source; see Fig. 1), resulting in lower shock speeds than would be obtained for the case of working surfaces driven into a stationary environment.

In the following sections, we will describe simple analytic and numerical approaches for determining the motion of inter-

nal perturbations in pressure matched jets. However, full numerical simulations of the time-dependent flow are necessary in order to carry out a detailed description of structures such as the radius of the jet as a function of position, or the internal working surfaces we have described above. We leave such calculations for future studies.

### c) Analytic Approach: Retarded Solutions

We consider a high Mach number, isothermal jet, in pressure balance with a homogeneous environment. For this simple flow, the equation of motion reduces to Burgers’s equation:

$$\frac{\partial u}{\partial t} + u \frac{\partial u}{\partial x} = 0, \quad (9)$$

where  $x$  is the distance measured along the axis of symmetry ( $x = 0$  corresponds to the injection point),  $u$  is the velocity along the axis of symmetry, and  $t$  is the time.

Burgers’s equation (see eq. [9]) allows discontinuous solutions. The solutions with discontinuous  $u$  show velocity jumps that travel with a velocity

$$v = \frac{1}{2}(u_1 + u_2), \quad (10)$$

where  $u_1$  and  $u_2$  are the pre- and postdiscontinuity velocities. These discontinuities correspond to the internal working surfaces described in the previous section (see eqs. [6], [7], and [8]). We should note that Burgers’s equation does not necessarily imply mass conservation, so that internal working surfaces in the jet (which expel gas sideways into the surrounding environment; see § IIb and Fig. 1) do not pose any particular problem for our one dimensional formulation. For a discussion of solutions to Burgers’s equation see, e.g., Whitham (1974, chap. 4).

It can also be shown that Burgers’s equation has a “retarded solution” given by

$$u(x, t) = u_0(t'), \quad (11)$$

where

$$u_0(t') = u(x = 0, t'), \quad (12)$$

and

$$t' = t - \frac{x}{u_0(t')} \quad (13)$$

is the retarded time. In other words, the velocity of the fluid parcel that at time  $t$  is at position  $x$  [i.e.,  $u(x, t)$ ] is equal to the velocity at the source [ $u_0(t')$ ] at the time  $t'$  (see eq. [13]) when the fluid parcel was ejected from the source. In the following, we will discuss an example in which this retarded solution (eqs. [11]–[13]) together with the jump condition (eq. [10]) can be used to obtain an analytic solution to the flow.

Let us consider a flow with initial conditions

$$u(x, t = 0) = U_0, \quad (14)$$

and a boundary condition at the source

$$u_0(t) = U_0; \quad t < 0, \quad (15a)$$

$$u_0(t) = U_0 + \alpha t; \quad t \geq 0. \quad (15b)$$

If we write the velocity in units of  $U_0$ , time in units of  $U_0/\alpha$ , and the distance in units of  $U_0^2/\alpha$ , the boundary conditions simplify

to

$$u_0(t) = 1 ; \quad t < 0 , \quad (15a)$$

$$u_0(t) = 1 + t ; \quad t \geq 0 . \quad (15b)$$

In these dimensionless variables, the criterion derived in the previous section indicates that a discontinuity should form at a time

$$t_s = 1 , \quad (16)$$

at a distance

$$d_s = 1 \quad (17)$$

from the jet source. We will now show that this criterion is indeed met by the analytic solution to Burgers's equation (eq. [9]). We find the analytic solution by solving equation (13) for the retarded time, using the velocity at the source given by equation (15b) to obtain

$$t' = \frac{1}{2}[t - 1 + \sqrt{(1+t)^2 - 4x}] \quad (18)$$

and from equation (11), we obtain

$$u(x, t) = \frac{1+t}{2} + \frac{1}{2}\sqrt{(1+t)^2 - 4x} ; \quad x < t , \quad (19a)$$

$$u(x, t) = 1 ; \quad x \geq t . \quad (19b)$$

In equation (19a) the positive sign for the root gives the physical solution. The solution given by equations (19a) and (19b) is well behaved for  $t < 1$ . However, for  $t > 1$ , this solution is double-valued (i.e., the point in which the parabola described by eq. [19a] joins the straight line described by eq. [19b] occurs in the lower, unphysical branch of the parabola). This is a result of the fact that at the time  $t_s = 1$ , a shock wave is formed. The initial position of the shock wave is at the place where the parabolic section of the velocity profile (eq. [19a]) joins the constant velocity section (eq. [19b]), this position corresponds to a distance  $d_s = 1$  from the injection point (in agreement with the criterion for the formation of discontinuities given by eqs. [16] and [17]). We note that a similar solution can be found for the case of a flow with a finite Mach number, in which the effects of pressure gradients can be important (Landau and Lifshitz 1978, § 94).

After the discontinuity is formed, it travels in the downstream direction with the velocity given by equation (10), which in this case can be written as

$$v = \frac{dx_s}{dt} = \frac{1}{2} [1 + u(x_s, t)] , \quad (20)$$

where  $u(x_s, t)$  is the velocity upstream of the discontinuity (the undisturbed downstream velocity is equal to 1; see eq. [15a]), which is given by equation (19a). Using equation (19a), equation (20) becomes a differential equation for the position  $x_s$  of the shock wave

$$\frac{dx_s}{dt} = \frac{3+t}{4} + \frac{1}{4}\sqrt{(1+t)^2 - 4x_s} . \quad (21)$$

It can be shown in a straightforward way that the solution to this equation is

$$x_s(t) = \frac{1}{4}\left(\frac{3}{4} + \frac{5}{2}t + \frac{3}{4}t^2\right) , \quad (22)$$

which satisfies the boundary condition  $x_s(t=1) = 1$ .

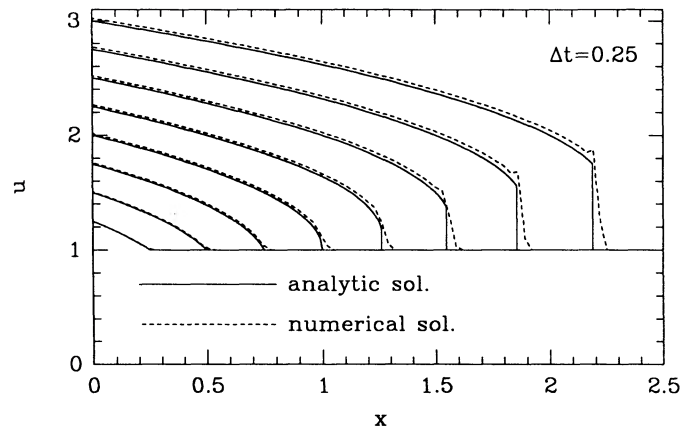


FIG. 2.—Analytic (solid lines) and numerical (dashed lines) solutions for the problem of a source with velocity increasing linearly with time (see § IIc). The solutions for times  $t = 0.25, 0.5, 0.75, 1.00, 1.25, 1.5, 1.75,$  and  $2.0$  are shown. The presence of a discontinuity for  $t > 1$  is clearly seen.

To summarize, for times  $t < 1$ , the velocity as a function of position is given by equations (19a) and (19b). At  $t = 1$ , a discontinuity appears at the position  $x_s = 1$  and then starts moving downstream as described by equation (22). For  $t > 1$  there are two smooth regions of the flow, separated by a discontinuous jump in the velocity. The solution for  $t > 1$  is given by

$$u(x, t) = \frac{1+t}{2} + \frac{1}{2}\sqrt{(1+t)^2 - 4x} ; \quad x < x_s(t) , \quad (23a)$$

$$u(x, t) = 1 ; \quad x \geq x_s(t) , \quad (23b)$$

where the position of the discontinuity,  $x_s(t)$ , is given by equation (22). In Figure 2, we plot the velocity field (i.e., velocity as a function of position) given by equations (19a) and (19b) and (23a) and (23b) for different times. The development of a discontinuity for  $t > 1$  can be clearly seen.

This solution illustrates the kind of flows that can be obtained by considering jets with time-varying injection velocities. In the simple case of a jet in which the source velocity increases at a constant rate, it is possible to obtain an analytic solution to Burgers's equation (as we have described above). However, for sources with more complex velocity variations, it is no longer possible to find analytic solutions in a straightforward way.

Because of this, in the following sections we present numerical solutions to Burgers's equation (eq. [9]) carried out with a flux-corrected McCormack method (which is described in detail by Raga and Böhm 1987). In order to illustrate the accuracy of the results obtained with this numerical method, in Figure 2, we show a comparison between the analytic solution described above and a numerical solution for the same flow.

We end this section by noting the following interesting property of the solutions to Burgers's equation. From observations of stellar jets (e.g., from high-resolution, long-slit spectra) one can determine the velocity of the flow as a function of position (after carrying out adequate corrections for the orientation of the flow with respect to the plane of the sky). The flow should be composed (of course, provided that the scenario proposed in this paper is indeed correct) of segments with smoothly varying velocity with position, separated by sudden jumps in the velocity (which would correspond to the discontinuities or "internal working surfaces" discussed above).

The smooth regions of the observed velocity/position curve (measured along the jet) can be described with a retarded solution (eqs. [11]–[13]). With the observed velocities and positions along these segments, it is in principle possible to reconstruct part of the history of the past variability of the jet source. For example, if we observe a jet velocity  $u_1$  at a distance  $x_1$  away from the source, this implies that at a time  $t_1 = x_1/u_1$  years ago the source had an outflow speed equal to  $u_1$ . This simple characteristic of the solutions to Burgers's equation gives us an in principle very powerful tool to explore the long-term time variability of the sources of stellar jets by observing the spatial velocity structure of the jets.

As discussed in § I, the velocity along the axis of symmetry can also be modified by the presence of internal shocks in the jet. For high Mach number jets, however, these velocity variations are very small (of the order of the sound speed). Supersonic velocity variations in the smooth regions of the observed velocity/position curve should indeed represent the time dependence of the source velocity. Detailed (axisymmetric) calculations of this kind of flow should also have this property. Our simplified approach (using Burgers's equation), however, only provides an approximate description of the motion of the working surfaces of a jet (which in principle can have very complex structures; see § IIb).

In this way, it is possible to reconstruct segments of the past history of the source variability, which correspond to the continuous segments of the observed velocity/position curve. However, the discontinuities observed in the velocity/position curves produce “gaps” in certain time intervals in the reconstructed history of the source variability (the gas ejected from the source during these time intervals has been “swallowed” by the corresponding working surface; see § IV). In § IV, we discuss an application of this technique to the case of the HH 46/47 jet.

### III. JETS WITH PERIODIC SOURCES

We now consider solutions to the problem of highly supersonic, pressure-matched isothermal jets from sources with more complex time-dependent behaviors. We first study a jet with initial conditions

$$u(x, t = 0) = 0, \quad (24)$$

and injection velocity

$$u_0(t) = 1 - \cos(2\pi t), \quad (25)$$

where the time is given units of the period  $\tau$  of the source oscillation, velocities are given in units of the half-amplitude  $U_0/2$  of the oscillation, and distances are given in units of  $U_0\tau/2$ .

The results of a numerical integration of these equations are shown in Figure 3 (where the velocity as a function of position is given at time intervals  $\Delta t = 0.5$ ). In this figure, we see that a first discontinuity is formed, and that it then travels away from the source. Successive discontinuities are formed, which travel faster than the first discontinuity (this is a result of the fact that these discontinuities are traveling into jet material which is already in motion away from the source). The second discontinuity eventually “catches up” with the first discontinuity (we see that this is about to happen in the plot corresponding to time  $t = 2.5$  in Fig. 3).

This calculation represents the solution that would be obtained for a source that is “turned on” at  $t = 0$ , thereafter having a time-dependent velocity as described by equation

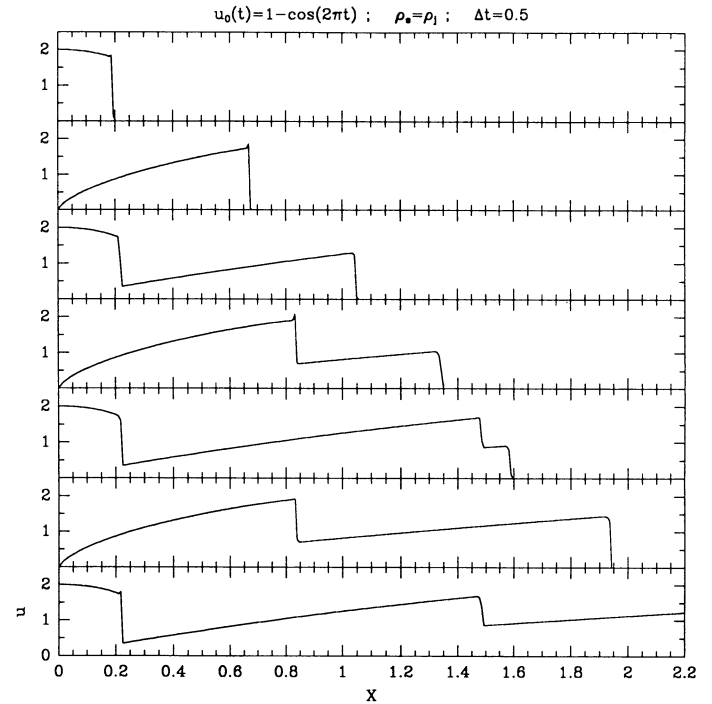


FIG. 3.—Velocity as a function of position for the  $\rho_e = \rho_j$  model (see § III). The solutions for  $t = 0.5$  (top), 1.0, 1.5, 2.0, 2.5, 3.0, and 3.5 (bottom) are shown.

(25). The leading discontinuity (see Fig. 3) corresponds to the “head” of the jet, and the successive discontinuities (that eventually overtake the head of the jet) correspond to internal working surfaces (as described in §§ II and III). As we have assumed a constant density in our derivation of the equation of motion, this solution corresponds to a jet traveling into an environment with density  $\rho_e = \rho_j$  (where  $\rho_e$  and  $\rho_j$  are the environment and jet densities, respectively).

We can also simulate the solution for a jet with a periodic source moving into a medium with a density  $\rho_e \ll \rho_j$ . This is done tracking the leading perturbation in the numerical calculation, and allowing it to move with the velocity of the flow upstream of the discontinuity (in the case of  $\rho_e = \rho_j$ , the leading perturbation moves at one-half of the upstream velocity; see eq. [5]). In Figure 4, we show the solution for a jet moving into an environment with a negligible density, and a time-dependent injection velocity given by

$$u_0(t) = 1 + \cos(2\pi t). \quad (26)$$

The solution is qualitatively similar to the one obtained for the high-density ( $\rho_e = \rho_j$ ; see Fig. 3) case, with the main difference that now the head of the jet “escapes.” In other words, the head of the jet always has a higher velocity than the following internal working surfaces, so that these never catch up with the jet head.

Jets with a density much smaller than the environmental density (i.e.,  $\rho_e \ll \rho_j$ ) will produce an almost stationary head, with the internal working surfaces hitting it periodically. This case is qualitatively similar to the  $\rho_e = \rho_j$  case and will not be further discussed.

The similarities and differences between the  $\rho_e = \rho_j$  and the  $\rho_e \ll \rho_j$  calculations are better illustrated in Figure 5. In this figure, we show constant- $u$  contours in the  $(x, t)$ -plane. The

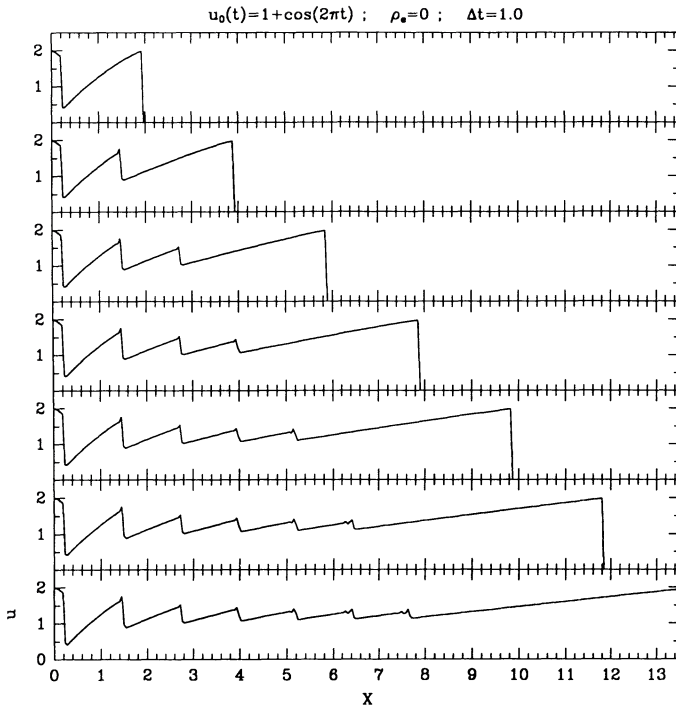


FIG. 4.—Velocity as a function of position for the  $\rho_e \ll \rho_j$  model (see § III). The solutions for  $t = 1.0$  (top), 2.0, 3.0, 4.0, 5.0, 6.0, and 7.0 (bottom) are shown.

discontinuities in the flow can be seen as lines of “piled up” contours, travelling away from the jet source (located at  $x = 0$ , see above).

It is clearly seen that in the  $\rho_e = \rho_j$  case (Fig. 5a) the successive internal working surfaces of the jet catch up with the head of the jet, while in the  $\rho_e \ll \rho_j$  case (Fig. 5b) the internal working surfaces never catch up with the head of the jet (which has a larger velocity). The other difference between the two solutions is a phase shift, which is a direct result of the chosen source oscillations (see eqs. [25] and [26]).

Except for the behavior close to the head of the jet and the phase shift (mentioned above), the solutions for the  $\rho_e = \rho_j$  and the  $\rho_e \ll \rho_j$  cases are very similar. In both cases, we see that the region close to the source (i.e., away from the head of the jet) develops a velocity structure that is periodic in both space and time. From Figures 5a and 5b, we see that in this region, the velocity of the internal working surfaces after a rapid acceleration reaches an approximately constant value  $v_{ws} \approx 1.25$  (measured in units of the half-amplitude  $U_0/2$  of the source oscillation; see above). The distance between internal working surfaces is also  $d_{ws} \approx 1.25$  (in units of  $U_0 \tau/2$ ), a result of the fact that the ratio  $d_{ws}/v_{ws}$  is equal to the period source oscillation. We also see that the head of the jet moves at a constant velocity  $v_H = 2.0$  for the  $\rho_e \ll \rho_j$  case (Fig. 5b), while for the  $\rho_e = \rho_j$  case (Fig. 5a) the head of the jet shows a variable velocity (with an average velocity of  $v_H \approx 0.66$ ).

From these results, we can conclude the following. Jets with sources that are “turned on” at a given time and thereafter have a periodically varying injection velocity, will show a “head” and one or more “internal working surfaces” traveling away from the source. We have studied two cases which show somewhat different characteristics:

1.—If the environmental density is much lower than the jet density (as illustrated in Fig. 5b), the head of the jet will show

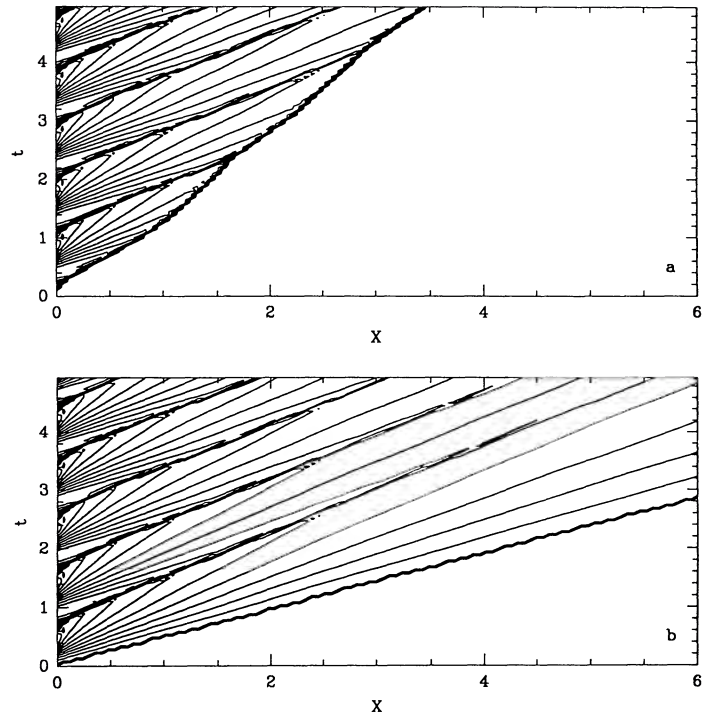


FIG. 5.—The solutions for the  $\rho_e = \rho_j$  (top) and  $\rho_e \ll \rho_j$  (bottom) models shown as constant velocity contours in the position/time ( $x, t$ ) plane (see § III). The equally spaced contours correspond to velocity differences of 0.2 (i.e., corresponding to 10% of the full amplitude of the source oscillation; see eqs. [25] and [26]).

larger proper motions and radial velocities than the internal working surfaces. From the case shown in Figure 5b, we obtained  $v_H \approx 1.6v_{ws}$ , though this value might be somewhat different for sources with periodic variations different from the one given by equation (26). Observations of such jets would be likely to show the head of the jet at a large distance from the source, and one or more internal working surfaces at a considerably smaller distance from the jet source.

2.—If the environmental density is comparable to or higher than the jet density, the internal working surfaces are faster than the head of the jet, and eventually catch up with the head. In our  $\rho_e = \rho_j$  calculation (see Fig. 5a), we find that  $v_H \approx 0.5v_{ws}$  (though this value could be somewhat different for source variations other than the one given by eq. [25]). Observations of such jets would be likely to show one or more internal working surfaces in the process of “catching up” with the head of the jet.

#### IV. COMPARISON WITH OBSERVATIONS OF HH 46/47

The Herbig-Haro object HH 46/47 appears to be one of the best candidates for an interpretation with our time-dependent source jet models. This object shows a well-aligned, jet like structure, with a bright condensation (HH 47A) at a distance of  $\sim 150''$  from the source (which is detected in the infrared; see, e.g., Emerson *et al.* 1984), and a considerably fainter, arclike structure (HH 47D) at a distance of  $\sim 230''$  from the jet source (see, e.g., Dopita, Schwartz, and Evans 1982). HH 47A and HH 47D have been interpreted as the result of two outflow episodes (Dopita, Schwartz, and Evans 1982; Hartigan, Raymond, and Meaburn 1990; Reipurth and Heathcote 1990).

Furthermore, the fact that observations of proper motions (Schwartz, Jones, and Sirk 1984), radial velocities (Graham and Elias 1983; Meaburn and Dyson 1987; Reipurth 1989a; Hartigan, Raymond, and Meaburn 1990), and time variability (Graham and Heyer 1989) are available in the literature makes the HH 46/47 system particularly interesting for a comparison with theoretical predictions.

In order to carry out a comparison with our model predictions, we have measured the radial velocity of the [S II] 6717 + 6731 emission as a function of position along the jet on the [S II] 6717 + 6731 position-velocity diagram of Reipurth and Heathcote (1990) (shown in the review of Reipurth 1989a). Actually, at distances  $< 120''$  from the source the line profiles show a strong component with a negative radial velocity of  $\sim 150\text{--}200 \text{ km s}^{-1}$ , and a much fainter component with approximately one-half of this velocity (see Meaburn and Dyson 1987; Reipurth 1989a). We have identified the velocity of the high-intensity component with the radial velocity of the jet (the fainter component might be coming from the boundary layer at the edges of the jet, as suggested by Meaburn and Dyson 1987).

In Figure 6, we show the velocity of the jet as a function of distance from the source (taken from the observations of Heathcote and Reipurth 1990; see also Reipurth 1989a). We have used the distance to HH 46/47 and the proper motion of HH 47A (Schwartz, Jones, and Sirk 1984 give a distance of 245 pc to the HH 46/47 system, and a proper motion velocity of  $159 \text{ km s}^{-1}$  for the northern part of HH 47A), together with the radial velocity of HH 47A measured on the spectrum of Reipurth (1989a) to determine an angle of  $\theta = 38^\circ$  between the axis of the HH 46/47 system and the plane of the sky. With the distance and orientation of the HH 46/47 system, it is then possible to calculate the actual spatial velocity of the emitting material as a function of distance from the source (see Fig. 6).

As has been noted by Reipurth (1989a) and by Hartigan, Raymond, and Meaburn (1990), this velocity versus position

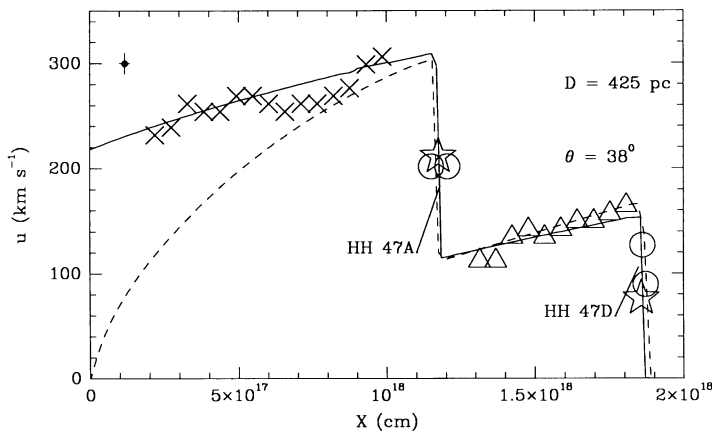


FIG. 6.—Velocity as a function of position for HH 46/47 as obtained from the observations of Reipurth 1989a, corrected for distance and projection effects. The triangles indicate the region interpreted as the first outflow episode, and the crosses indicate the second outflow episode. The circles indicate the positions of HH 47A and HH 47D, which are interpreted as working surfaces in the jet flow (see § IV). The errors in the position and velocity determinations are indicated by the dot with error bars in the upper left-hand corner of the graph. The dashed line corresponds to the predictions from the “cosine source” model and the solid line to the predictions from the “sawtooth source” model (see § IV and Table 1). The starred points correspond to the velocities predicted from the models for the two working surfaces of the jet (see § IV).

configuration (see Fig. 6) suggests the existence of two outflow episodes. The first outflow episode would have produced the low velocity region between  $x = 1.3$  and  $1.9 \times 10^{18} \text{ cm}$  (see Fig. 6), and the second outflow episode would have produced the high-velocity,  $x < 1.2 \times 10^{18} \text{ cm}$  region.

Accordingly, we model the HH 46/47 system with our simplified model by assuming that the source has been “turned on” sometime in the past and has since had two outflow episodes. These outflow episodes are to be characterized by an initial increase in the source velocity, followed by a subsequent drop in the source velocity. The density of the jet at the injection point is assumed to be constant with time.

We have used two different assumptions for the source variability. In the first case, we assume that the source is “turned on” at full velocity, and that is thereafter varies following a cosine law  $u_0(t) = 0.5U_0\{1 + \cos [2\pi(t - t_0)/\tau]\}$ . In the second case, we assume that the source has a “sawtooth” variability (the source is turned on at full velocity  $U_0$ , the source velocity then decreases linearly, and when it reaches zero velocity, the second “spike” of the sawtooth is reached). We assume that the environment has a density  $\rho_e = \rho_j$  (where  $\rho_j$  is the constant jet density).

We attempt to fit the velocity versus position structures predicted from these models (equivalent to those shown in Figs. 3 and 4) to the observations of HH 46/47. Our two assumed forms for the source variability have three free parameters: the time  $t_0$  at which the source was initially turned on ( $t = 0$  is taken to correspond to the time at which the observations of HH 46/47 were obtained), and the period  $\tau$  and amplitude  $U_0$  of the subsequent oscillation. We fix these parameters by fitting the positions and amplitudes of the two “jumps” (which correspond to HH 47A and HH 47D, see above) in the observed velocity versus position dependence of HH 46/47.

We show a comparison of the model predictions obtained in this way with the observations of HH 46/47 in Figure 6. Both the “cosine” and the “sawtooth” models fit well the positions and velocity jumps of the observed “velocity discontinuities”. The parameters needed in order to obtain these fits are given in Table 1.

Even though the two models described above do reproduce the observed jumps in the velocity versus position diagram of HH 46/47, it is clear that the general characteristics of the smooth regions of the observed velocity/position dependence are better reproduced by the “sawtooth source” model (see Fig. 6). Because of this, one might conclude that the “sawtooth source” model better represents the actual time dependence of the source of the HH 46/47 jet. However, these fits are based on the agreement of the observed and predicted positions of the working surfaces of the jet. The fact that our simplified models

TABLE 1

MODEL PARAMETERS FOR THE COMPARISON WITH HH 46/47

Model <sup>a</sup>	$t_0(\text{yr})^b$	$\tau(\text{yr})^c$	$U_0(\text{km s}^{-1})^d$
“Cosine source” .....	−5575	2787	318
“Sawtooth source” ...	−6415	4612	357

<sup>a</sup> Models with both a cosine and a sawtooth source velocity variability have been computed (see text).

<sup>b</sup>  $t_0$  is the time at which the source was “turned on” for the first time ( $t = 0$  corresponds to the time at which the observations of HH 46/47 were carried out).

<sup>c</sup>  $\tau$  is the period of the source velocity oscillation.

<sup>d</sup>  $U_0$  is the full amplitude of the source velocity oscillation.

do not accurately predict the motion of the working surfaces (see § IIc) introduces a large uncertainty in the comparison between the theoretical predictions and the observations.

This result can also be seen in another way. As we have noted in § IIc, it is possible to reconstruct the source variations from the velocity versus position observed along a stellar jet, by making use of the “retarded solution” which is characteristic of Burgers’s equation. For each point for which we have measured the velocity along the HH 46/47 outflow, we can calculate the time  $t = -x/u$  (where  $x$  is the distance from the source, and  $u$  is the jet velocity at this position) at which the material left the source. At that time, the source velocity had a value  $u_0 = u$  (see the discussion in § IIc). In this way, we can reconstruct the time-dependent source velocity  $u_0(t)$ .

The result of this calculation is shown in Figure 7, where it can be clearly seen that the HH 46/47 jet actually corresponds to two episodes of active outflow. The region of the flow between the source and HH 47A (see Fig. 6) has been ejected from the source in a period from 1000 yr ago to the present time at velocities of  $\approx 300\text{--}240\text{ km s}^{-1}$ . The region between HH 47A and HH 47D apparently corresponds to the “tail” (with velocities  $\sim 100\text{--}180\text{ km s}^{-1}$ ) of a previous outflow episode which ended approximately 1500–2500 yr ago. The information of the source variability from  $\sim 3000\text{--}1000$  yr ago (see Fig. 8) has been lost, because the “internal working surface” corresponding to HH 47A has “swallowed” (and ejected sideways into the cocoon of the jet; see § IIb) the jet material that was ejected from the source during this time period. The information of the source variability for times longer than 4000 yr ago has been lost due to the effect of the working surface corresponding to HH 47D.

In Figure 7, we also show the “cosine” and “sawtooth” source variations that were necessary for reproducing the observed positions and amplitudes of the velocity jumps corresponding to HH 47A and D (see above and Fig. 6). It is clear

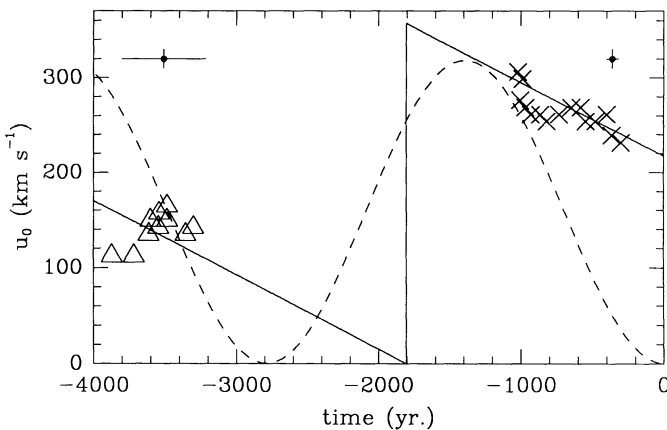


FIG. 7.—The reconstructed history of the past time variability of the HH 46/47 source velocity. The triangles correspond to the first outflow episode, and the crosses correspond to the second outflow episode (see Fig. 6 and § IV). The errors in the determinations of the time and the velocity are given by the dots with error bars in the upper right-hand and left-hand corners of the graph (which correspond to the data points indicated with crosses and with triangles, respectively). We note that the large errors in the time determination for the first outflow episode (triangles) result in apparent inversions of the time sequence at which successive regions along the jet were ejected. The solid and dashed lines correspond to the source velocity variability used for the “sawtooth” and “cosine” models, respectively (see Fig. 7, Table 1, and § IV). It is clear that the sawtooth model reproduces the data points much better than the cosine model.

that the sawtooth curve better reproduces the empirically determined velocity variability of the source.

We also note the following two interesting results:

1.—As we have described in § IIb, internal working surfaces differ from the head of the jet in that their associated shock velocities are lower. From our simple, constant density model, we would conclude that the emission observed in HH 47A would mainly come from two shocks of velocity  $v_s = \frac{1}{2}(u_1 - u_2)$  (see Fig. 1 and eq. [17]), where  $u_1$  and  $u_2$  are the velocities of the flow before and after the velocity jump associated with HH 47A. From Figure 6b, we see that this velocity is  $v_s \approx 90\text{ km s}^{-1}$ . This rather low shock velocity might help to explain the low excitation observed for the spectrum of HH 47A (see, e.g., Dopita, Schwartz, and Evans 1982), a fact that has always been a problem for the interpretation of HH 47A as the head of a jet (see, e.g., Raga and Mateo 1987). A similar idea for a possible solution to the problem of the low excitation of HH 47A has recently been suggested by Hartigan, Raymond, and Meaburn (1990). The fact that the condensation HH 47D has a higher excitation than HH 47A (as indicated by the spectrophotometric observations discussed above) does not agree with the predictions from our model (in which the shock velocities associated with the two working surfaces are similar). This observation indicates that the environment ahead of HH 47D possibly has a lower density than the HH 46/47 jet (while  $\rho_e = \rho_j$  was assumed in our model).

2.—It is also interesting that the velocity of HH 47A has a value similar to the average of the pre- and postdiscontinuity values of the jet velocity. This is exactly what is to be expected for internal working surfaces in a jet with constant density [which have a velocity  $v = \frac{1}{2}(u_1 + u_2)$ ; see eq. [7]]. This agreement between the observed and predicted velocities for HH 47A (see Fig. 6) represents a partial empirical justification of our assumption of a constant density for our jet models (see § IIb).

To summarize, we find that with our time-dependent source jet models it is indeed possible to reproduce the velocity versus position distribution observed for HH 46/47. These models can also explain the velocity and (at least in a qualitative way) the low excitation of the condensation HH 47A. We also find that it is possible to partially reconstruct the past velocity variability of the HH 46/47 source, showing evidence for two outflow episodes (a recent outflow, extending from 1000 yr ago to the present, and a previous outflow, which ended approximately 1500–2500 yr ago; see Fig. 6).

## V. CONCLUSIONS

We have presented models for high Mach number, isothermal, pressure-matched jets ejected from sources with variable velocities. We find that variations in the source velocity induce the formation of discontinuities in the jet which can be described as “internal working surfaces.”

Sources with periodic variations produce jets with a “head” which is followed by one or more “internal working surfaces.” If the jet is moving into a low-density environment, the head of the jet has a higher velocity than the internal working surfaces, so that a configuration of a fast condensation (i.e., the head of the jet) far away from the source and several slower (and fainter) condensations closer to the source will eventually develop. This kind of configuration in principle might explain the condensation structure, position/velocity diagrams, and proper motions observed by Reipurth (1989a) for the HH 34 jet

(but we leave a more detailed study of this possibility for the future). A similar scenario has been suggested by Rees (1978) for the case of extragalactic, relativistic jets. This scenario, however, by no means represents the only possible mechanism for the formation of knots in astrophysical jets (see, e.g., Blondin, Fryxell, and Königl 1990).

However, if the jet is moving into a high-density environment, internal working surfaces move faster than, and eventually catch up with the head of the jet. This configuration appears to be relevant for modeling objects such as HH 46/47. The stellar jet HH 111 (Reipurth 1989a), which shows two well-aligned bow shock-like structures in each outflow direction is also a good candidate for an interpretation in terms of our models.

We have attempted to model the spatially resolved velocity structure of the HH 46/47 outflow with our jet models. We find that it is indeed possible to reproduce the observations by choosing an appropriate time variability for the jet source. This surprising (due to the simplicity of our models) agreement strengthens the evidence for time-dependent outflow velocities in the source of Herbig-Haro objects.

Our approximate treatment of the flow equations also provides a simple way for reconstructing the past time variability of the source velocity from the velocity versus position structure observed in the jet. We have done this for the case of HH 46/47, and we find evidence that the source of this object has had a decline in outflow velocity from  $\approx 300$  to  $240 \text{ km s}^{-1}$  during the last 1000 yr. We also detect the "tail" of a previous outflow episode (with velocities  $\sim 100\text{--}180 \text{ km s}^{-1}$ ) which ended approximately 1500–2500 yr ago.

It appears that this previous outflow episode might have started approximately 6400 yr ago, leading to an estimate for the period between the two outflow episodes of the order of 4600 yr. This estimate, however, is based on a comparison with models in which it was assumed that the jet initially moves into a stationary environment with  $\rho_e = \rho_j$  (where  $\rho_e$  and  $\rho_j$  are the environmental and jet densities, respectively). A different assumption for the value of the environmental density would lead to somewhat different estimates for this period.

If this interpretation of the HH 46/47 system is correct, it implies a variability of the source in a time scale  $\tau \sim 4500$  yr (see Table 1 and § IV) previously unobserved in young stars. As has been pointed out by Hartigan, Raymond, and Meaburn (1990), such a time scale is most similar to the time scale of  $\sim 5 \times 10^3$  yr between FU Orionis outbursts estimated by

Herbig (1977, 1989). However, it is not clear whether or not the fact that the time scales agree well is sufficient to identify the variability of the HH 46/47 source with FU Orionis outbursts. The interpretation of stellar outflows as eruptive events was first proposed by Dopita (1978), and Reipurth (1985) has discussed in detail the possible relation between H-H objects and FU Orionis outbursts.

Winds from FU Orionis stars are characterized by mass-loss rates  $\sim 10^{-5}$  to  $10^{-4} M_{\odot} \text{ yr}^{-1}$  (Croswell, Hartmann, and Avrett 1987), which are three to four orders of magnitude larger than the mass-loss rates of T Tauri winds. The velocities of FU Orionis winds ( $\sim 300\text{--}400 \text{ km s}^{-1}$ ) do not seem to differ (at least in order of magnitude) from the velocities of T Tauri winds. This does not seem to be in such good agreement with our models, for which a time-dependent initial jet velocity is necessary. However, we should note that the observations do not rule out the relatively small variations in the wind velocity that would be necessary for the formation of internal working surfaces in stellar jets (see § IIa). It is also unclear whether or not large variations in the mass-loss rate (but with an approximately constant wind velocity) might result in variations of the velocity of the jet formed by the collimation of such a wind. Though simple arguments indicate that the dependence of the jet velocity on the mass-loss rate (for a constant wind velocity) probably is not very large (Raga and Cantó 1989b), a detailed study of time-dependent effects in stellar wind collimation models would be necessary in order to answer this question in a more conclusive way.

From these arguments we conclude that it is unclear whether or not the variability of the HH 46/47 source (deduced from the kinematic structure of the HH 46/47 jet) corresponds to past FU Orionis events. However, this possible new link between FU Orionis eruptions and the formation of HH objects presents an extremely interesting possibility that should be explored in future work (also see the discussions of Reipurth 1989a, and Hartigan, Raymond, and Meaburn 1990).

A large part of this work was carried out in the 2nd PITA workshop, which took place in Venezuela. L. B., J. C., and A. R. would like to thank the students and staff of CIDA for their hospitality during their stay in Mérida. This work was partially supported by the DGAPA (UNAM) grant number IN-01-05-89 and by the Connaught Fund of the University of Toronto and the Natural Sciences and Engineering Research Council of Canada.

#### REFERENCES

- Biro, S. 1990, B.Sc. thesis, Universidad Nacional Autónoma de México.  
 Blondin, J. M., Fryxell, B. A., and Königl, A. 1990, *Ap. J.*, **360**, 370.  
 Blondin, J. M., Königl, A., and Fryxell, B. A. 1989, *Ap. J. (Letters)*, **337**, L37.  
 Bührke, T., Mundt, R., and Ray, T. P. 1988, *Astr. Ap.*, **200**, 99.  
 Cantó, J. 1980, *Astr. Ap.*, **86**, 327.  
 Cantó, J., Raga, A. C., and Binette, L. 1989, *Rev. Mexicana Astr. Af.*, **17**, 65.  
 Cantó, J., Tenorio-Tagle, G., and Różycka, M. 1988, *Astr. Ap.*, **192**, 287.  
 Croswell, K., Hartmann, L., and Avrett, E. H. 1987, *Ap. J.*, **312**, 227.  
 Dopita, M. A. 1978, *Ap. J. Suppl.*, **37**, 117.  
 Dopita, M. A., Schwartz, R. D., and Evans, I. 1982, *Ap. J. (Letters)*, **263**, L73.  
 Dyson, J. E. 1987, in *IAU Symposium 122, Circumstellar Matter*, ed. I. Appenzeller and C. Jordan (Dordrecht: Reidel), p. 159.  
 Emerson, J. P., Harris, S., Jennings, R. E., Beichman, C. A., Baud, B., Beintema, D. A., Marsden, P. L., and Wesselius, P. 1984, *Ap. J. (Letters)*, **278**, L49.  
 Graham, J. A., and Elias, J. H. 1983, *Ap. J.*, **272**, 615.  
 Graham, J. A., and Heyer, M. 1989, *Pub. A.S.P.*, **101**, 573.  
 Hartigan, P. 1989, *Ap. J.*, **399**, 987.  
 Hartigan, P., Raymond, J., and Meaburn J. 1990, *Ap. J.*, **362**, 624.  
 Heathcote, S., and Reipurth, B. 1990, *Ap. J.*, submitted.  
 Herbig, G. H. 1977, *Ap. J.*, **217**, 693.  
 ———. 1989, in *Proc. of the ESO Workshop on Low Mass Star Formation and Pre-Main Sequence Objects*, ed. B. Reipurth (Garching bei München: ESO), p. 233.  
 Königl, A. 1982, *Ap. J.*, **261**, 115.  
 Landau, L. D., and Lifshitz, E. M. 1978, *Fluid Mechanics* (Oxford: Pergamon), §94.  
 Mundt, R., Brugel, E. W., and Bührke, T. 1987, *Ap. J.*, **319**, 275.  
 Meaburn, J., and Dyson, J. E. 1987, *M.N.R.A.S.*, **225**, 836.  
 Raga, A. C. 1988, *Ap. J.*, **335**, 820.  
 Raga, A. C., Binette, J., and Cantó, J. 1990, *Ap. J.*, **360**, 612.  
 Raga, A. C., and Böhm, K. H. 1987, *Ap. J.*, **323**, 193.  
 Raga, A. C., and Cantó, J. 1989a, *Ap. J.*, **344**, 404.  
 ———. 1989b, in *IAU Colloquium 120, Structure and Dynamics of the Interstellar Medium*, ed. G. Tenorio-Tagle, M. Moles, and J. Melnick (Berlin: Springer-Verlag), p. 276.  
 Raga, A. C., and Mateo, M. 1987, *A.J.*, **94**, 684.  
 Rees, M. J. 1978, *M.N.R.A.S.*, **184**, 61P.  
 Reipurth, B. 1985, *Astr. Ap.*, **143**, 435.

- Reipurth, B. 1989a, in *Proc. of the ESO Workshop on Low Mass Star Formation and Pre-Main Sequence Objects*, ed. B. Reipurth (Garching bei München: ESO), p. 247.
- . 1989b, *Astr. Ap.*, **220**, 249.
- Reipurth, B., Bally, J., Graham, J. A., Lane, A., and Zealy, W. J. 1986, *Astr. Ap.*, **164**, 51.
- Reipurth, B., and Heathcote, S. 1990, in preparation.
- Schwartz, R. D. 1975, *Ap. J.*, **195**, 631.
- Schwartz, R. D., Jones, B. F., and Sirk, M. 1984, *Astr. Ap.*, **89**, 1735.
- Silvestro, G., Ferrari, A., Rosner, R., Trussoni, E., and Tsinganos, K. 1987, *Nature*, **325**, 228.
- Tenorio-Tagle, G. 1989, in *IAU Colloquium 120, Structure and Dynamics of the Interstellar Medium*, ed. G. Tenorio-Tagle, M. Moles, and J. Melnick (Berlin: Springer-Verlag), p. 264.
- Wilson, M. J. 1984, *M.N.R.A.S.*, **209**, 923.
- Whitham, G. V. 1974, *Linear and Nonlinear Waves* (New York: Wiley Interscience).

LUC BINETTE and ALEJANDRO RAGA: Canadian Institute for Theoretical Astrophysics, McLennan Physical Laboratories, University of Toronto, 60 St. George Street, Toronto, Ontario, M5S 1A1

JORGE CANTÓ: Instituto de Astronomía, Universidad Nacional Autónoma de México, Apartado Postal 70-264, 04510 México, D. F., México

NURIA CALVET: Centro de Investigaciones de Astronomía, Apartado Postal 264, Mérida 5101-A, Venezuela